Data-Driven Tracking Control Design With Noisy Data and its Application in DC Microgrid Control

Zi-Jie Wei, Kun-Zhi Liu, Ping Lin, *Member, IEEE*, and Xi-Ming Sun, *Senior Member, IEEE*

***Abstract*—This article focuses on data-driven analysis and dynamic feedback tracking controllers design solely utilizing noisy measured data. By leveraging data-based representations, we establish data-based stability conditions for discrete-time systems. Then, we propose the data-based method for designing zero steady-state error tracking controller gains to achieve set-point tracking with guarantees of asymptotic stability, bypassing mathematical modeling of the controlled plant. Furthermore, considering the robustness against both the noise during data acquisitions and the disturbance affecting closed-loop operations, we develop a data-based H_∞ tracking control design method, ensuring that the closed-loop system satisfies the H_∞ performance. Finally, we apply the presented approaches to dc–dc converters control in dc microgrids. Voltage control of a single converter and power sharing of parallel-connected dc–dc converters are implemented by simulations and hardware experiments. The results show that the dc-bus voltage keeps stability under the input voltage disturbance and the load change. Through the droop control, the currents of the converters are adjusted as expected, which confirms the effectiveness of the proposed methods.**

***Index Terms*—DC–DC converters, data-driven tracking control, noisy data, stability analysis.**

I. Introduction

With the growing complexity of systems, establishing a mathematical model that meets expectations from first principles becomes increasingly laborious [1], such as power systems and urban transportation networks. In contrast, the abilities of data acquisition, transmission, and saving have grown more powerful with the development of information technologies. In recent years, data-driven is a hot topic in the field of system analysis and control. On the one hand, data of measured trajectories can be used to construct a mathematical model of the plant, followed by model-based analysis and control, as called the indirect method [2]. Typical indirect data-driven methods include system identification based on the least squares method [3], artificial neural network modeling [4], [5], etc. On the other hand, control laws can be obtained directly from data, bypassing mathematical modeling of the controlled plant. One of the direct data-driven frameworks worth mentioning is based on Willems' fundamental lemma [6], where the system is represented implicitly by the Hankel matrix of system trajectories. Fruitful results cover optimal control [1], [7], predictive control [8], [9], and linear quadratic regulation [1], [10], etc. Considering the noise affecting measured data, another data-based representation is from the robust control perspective. Specifically, a set of model parameters explaining the noisy data of system trajectories is constructed in the form of quadratic matrix inequality (QMI), which contains the true system. Building upon the matrix S-lemma [11] or the full-block S-procedure [12], stability analysis and control design can be developed for all systems of the set through measurements and the noise bound. Some efforts encompass aperiodic sampling control [13], [14], robust control [15], [16], event-triggered control [17], distributed control [18], autoregressive systems control [19], and so on.

In the context of the above QMI-based data-driven control design methods, many of them take the noise of data measured offline into account, while external disturbances that affect system dynamics are ignored. In [20], considering the disturbances during data sampling and closed-loop operations, $\mathcal{L}_2$-stability conditions are established. However, the aforementioned data-based results mainly focus on the stabilization problem, i.e., modifying the system behavior by the proportional feedback controller to achieve stability around a certain steady-state point. In this case, changes of the steady-state points may lead to static errors. Ref. [9] provides a data-driven model predictive control (MPC) approach, also called data-enabled predictive control (DeePC) in [21], which may suffer a large computational burden for complex systems. The authors in [7] studied optimal tracking control by solving an optimization problem offline with linear matrix inequality (LMI) constraints, but under the assumption of noiseless historical data. In contrast, we present a data-based method to design the tracking controller gains through offline noisy measurements. The authors in [16] proposed a dual-system approach to designing tracking controllers that guarantee H_2 performance for continuous-time systems. Given the application of digital control to power converters [22], we derive data-driven conditions for discrete-time systems.

DC microgrids have gained increasing attention in the last years, in virtue of efficiency, flexibility, and scalability [23], [24].

Received 13 February 2025; revised 6 May 2025 and 3 July 2025; accepted 1 August 2025. Date of publication 4 August 2025; date of current version 8 September 2025. This work was supported in part by the National Natural Science Foundation of China under Grant 08120005, Grant 08120010, and Grant 62203085, and in part by the Liaoning Revitalization Talents Program under Grant 04070204. Recommended for publication by Associate Editor A. Davoudi. *(Corresponding author: Kun-Zhi Liu.)*

The authors are with the Key Laboratory of Intelligent Control and Optimization for Industrial Equipment of Ministry of Education, Dalian University of Technology, Dalian 116024, China, and also with the School of Control Science and Engineering, Dalian University of Technology, Dalian 116024, China (e-mail: zijiewei@mail.dlut.edu.cn; kzliu1989@dlut.edu.cn; dmulinping@dlut.edu.cn; sunxm@dlut.edu.cn).

Color versions of one or more figures in this article are available at https://doi.org/10.1109/TPEL.2025.3595863.

Digital Object Identifier 10.1109/TPEL.2025.3595863

Stability analysis and control of dc microgrids are extremely important issues that need to be dealt with [25]. However, increasing the number of power devices leads to more variables and equations, resulting in a significantly more complex dc microgrid model [26]. Moreover, circuit parameter mismatch caused by measurement errors, electrical component aging [27], possible temperature drift [28], and topology parameter variations, may make it difficult for the controllers designed by establishing ideal state-space averaging models [29] to achieve the desired control performance. The authors in [30] and [31] adopted a two-step (in-direct) approach. Specifically, the converter dynamics are identified as a local model network or kernel basis functions first, and local linear controllers or model reference adaptive control algorithms are designed later. Similar ideas in the frequency domain are reflected in [32]. Compared with the two-step approaches, the direct data-driven methods can extract dynamic characteristics from experimental data directly without system identification. In [26], a passivity-based data-driven control design method is proposed, where dc microgrids are in the form of autoregressive systems and noiseless data are utilized. In [33], a DeePC algorithm for power converters was presented, where the effects of the noise were eliminated by using a larger dataset. However, it may lead to a high-dimension optimization problem and thus the algorithm may not be scalable to high-order systems. Besides, many DeePC methods are applied in power converters secondary control to adjust the power setpoints in [34], and auxiliary control to achieve the functionality of oscillation damping in [21] and [33], while this article focuses on the converters primary control with high frequency. In a nutshell, the main contributions of this article are summarized as follows.

1) For one thing, by merely utilizing noisy data of system trajectories measured in an offline experiment, a data-driven zero steady-state error tracking (ZSET) control method is proposed to realize set-point tracking with a rigorous guarantee of asymptotic stability. The controller gains are computed by solving a data-guided LMI. The measurement noise is reasonably assumed to be bounded.
2) For another, given the external disturbances that affect not only the measurement accuracy but also the system dynamics, a data-driven design method for the H_∞ tracking controller is established without the need for explicit system identification. The proposed results are applied to dc–dc converters control in dc microgrids, and verified by simulations and hardware experiments.

The rest of this article is organized as follows. The system description and the data-based representation in QMI forms are introduced in Section II. Section III presents the main results including data-based stability conditions and data-driven control algorithms for dc–dc converters in dc microgrids. Section IV provides the simulated and experimental results. Finally, Section V concludes this article.

Notations: Symbols $\mathbb{N}_0$ and $\mathbb{N}_+$ represent the sets of all nonnegative integers and positive integers, respectively. Symbols $\mathbb{R}^n$ and $\mathbb{R}^{n\times m}$ represent the sets of all n-dimensional vectors and $n\times m$ real matrices, respectively. The notation col$\{\dots\}$ denotes column vectors. The notations $P\succ 0$ ($P\succeq 0$) and $P\prec 0$ ($P\preceq 0$) indicate that matrix P is positive (semi-) definite and negative (semi-) definite, respectively. The notation sym$\{P\}$ represents $P+P^{\mathrm{T}}$. I denotes the identity matrix and 0 denotes the null matrix. $\|\cdot\|$ denotes the Euclidean vector norm. The symbol $\star$ indicates entries that can be inferred from symmetry. The symbol diag$\{\cdots\}$ represents a matrix where all elements outside the main diagonal are zero.

II. Preliminaries

A. System Description

Consider the discrete-time LTI system described by

$$\begin{aligned} x(k+1) &= Ax(k)+Bu(k)+B_d d(k)\\ y(k) &= Cx(k) \end{aligned} \tag{1}$$

where $k\in\mathbb{N}_0$, $x(k)\in\mathbb{R}^n$ denotes the state with initial value $x(0)=x_0$, $u(k)\in\mathbb{R}^m$ denotes the input, $y(k)\in\mathbb{R}^p$ denotes the output, $d(k)\in\mathbb{R}^{m_d}$ is the external disturbance. Matrices A, B, C and B_d are constant with appropriate dimensions. The state matrix A and input matrix B are entirely unknown.

One of the purposes of this paper is to design a ZSET controller to achieve that the output $y(k)$ of system (1) asymptotically tracks the desired set-point vector $r(k)\in\mathbb{R}^p$ in the absence of external disturbances, i.e., $d(k)\equiv 0$, without prior knowledge of system parameters. For another, in the presence of external disturbances, under the zero-initial condition, given a scalar $\gamma>0$, the closed-loop system with the designed H_∞ tracking controller achieves the H_∞ output tracking performance index γ, i.e.,

$$\sum_{k=k_0}^{\infty}\|y(k)-r(k)\|^2\le\gamma^2\sum_{k=k_0}^{\infty}\|\bar{d}(k)\|^2 \tag{2}$$

where $\bar{d}(k)=d(k)-d_s\in l_2[0,\infty)$, d_s is the steady-state values of $d(k)$.

To this end, the dynamic feedback tracking controller is given as

$$u(k)=K_1x(k)+K_2z(k) \tag{3}$$

where $z(k)\in\mathbb{R}^p$ is the integrator state vector satisfying

$$z(k+1)=z(k)+y(k)-r(k) \tag{4}$$

with $z(0)=0$.

In the absence of $d(k)$, the dynamic feedback tracking controller (3) is a ZSET controller. Define that x_s, u_s, y_s, and z_s are the known steady-state values, where $y_s=r(k)$ for $k\to+\infty$. The asymptotic stability means that $\bar{y}(k)\triangleq y(k)-y_s\to 0$ as $k\to+\infty$. The definitions of $\bar{x}(k)$, $\bar{u}(k)$ and $\bar{z}(k)$ are similar to $\bar{y}(k)$. When dealing with external disturbances, the dynamic feedback tracking controller (3) is used as the H_∞ tracking controller.

Based on the above definitions, the deviation equations are presented as

$$\begin{aligned} \bar{x}(k+1) &= A\bar{x}(k)+B\bar{u}(k)+B_d\bar{d}(k),\\ \bar{y}(k) &= C\bar{x}(k) \end{aligned} \tag{5}$$

and

$$\bar{u}(k) = K_1\bar{x}(k) + K_2\bar{z}(k), \tag{6}$$

$$\bar{z}(k+1) = \bar{z}(k) + \bar{y}(k). \tag{7}$$

Therefore, the augmented closed-loop system can be established as

$$\xi(k+1) = \bar{A}\xi(k) + \bar{B}\bar{K}\xi(k) + \bar{B}_d\bar{d}(k) \tag{8}$$

where $\xi(k) = \begin{bmatrix}\bar{x}(k)\\ \bar{z}(k)\end{bmatrix}$, $\bar{A} = \begin{bmatrix}A & 0\\ C & I\end{bmatrix}$, $\bar{B} = \begin{bmatrix}B\\ 0\end{bmatrix}$, $\bar{K} = [K_1, K_2]$, $\bar{B}_d = \begin{bmatrix}B_d\\ 0\end{bmatrix}$.

Remark 1: In virtue of the integrator state vector $z(k)$, the controller (3) is capable of zero steady-state error tracking. Traditional controller design methods depend on the explicit model, which may not go well when system identification is hard to achieve smoothly for the noisy data [35]. In what follows, a data-based representation is introduced for purely data-driven analysis and control.

B. System Representation From Noisy Data

Suppose that there are measurements $\{x(i)\}_{i=k_0}^{k_0+N}$ and $\{u(i)\}_{i=k_0}^{k_0+N-1}$, $k_0 \in \mathbb{N}_0$, $N \in \mathbb{N}_+$, sampled from the moment k_0 of the system

$$x(k+1) = Ax(k) + Bu(k) + B_w w(k),\ x(0) = x_0. \tag{9}$$

In the absence of external disturbances, the term $w(k) \in \mathbb{R}^{m_d}$ leads to the noise-corrupted measurement in a open-loop experiment offline [13]. In this case, the system (9) is the data sampling form of the system (1) for $d(k) \equiv 0$. Thus, the dynamic of the augmented closed-loop system can be described by

$$\xi(k+1) = \bar{A}\xi(k) + \bar{B}\bar{K}\xi(k). \tag{10}$$

When considering external disturbances, the noise term $w(k)$ accounts for both the accuracy of offline data acquisition and the online operation of closed-loop systems. In order to achieve data-based H_∞ control design with noisy data for system (9), the H_∞ output tracking performance (2) is modified to

$$\sum_{k=k_0}^{\infty} \|y(k) - r(k)\|^2 \le \gamma^2 \sum_{k=k_0}^{\infty} \|\bar{w}(k)\|^2 \tag{11}$$

where $\bar{w}(k)$ is similarly defined as $\bar{d}(k)$. In this case, the augmented closed-loop system (8) is modified to

$$\xi(k+1) = \bar{A}\xi(k) + \bar{B}\bar{K}\xi(k) + \bar{B}_w\bar{w}(k) \tag{12}$$

where $\bar{B}_w = \begin{bmatrix}B_w\\ 0\end{bmatrix}$.

The data matrices of (9) are defined as

$$\begin{aligned} X_+ &:= [x(k_0+1), x(k_0+2)\cdots x(k_0+N)],\\ X &:= [x(k_0), x(k_0+1)\cdots x(k_0+N-1)],\\ U &:= [u(k_0), u(k_0+1)\cdots u(k_0+N-1)],\\ W &:= [w(k_0), w(k_0+1)\cdots w(k_0+N-1)]. \end{aligned}$$

Among them X and U can be measured generally. Obviously, it holds that

$$X_+ = AX + BU + B_w W. \tag{13}$$

Rather than the statistical information required in system identification, a quite general and flexible assumption of the noise is given as follows [11].

Assumption 1: The noise sequence $\{w(i)\}_{i=k_0}^{k_0+N-1}$ collected in the matrix W satisfies $W \in \mathcal{W}$ with

$$\mathcal{W} := \left\{ W \in \mathbb{R}^{m_d\times N} \middle| \begin{bmatrix} W^{\mathrm{T}}\\ I\end{bmatrix}^{\mathrm{T}} \begin{bmatrix} Q_w & S_w\\ S_w^{\mathrm{T}} & R_w\end{bmatrix} \begin{bmatrix} W^{\mathrm{T}}\\ I\end{bmatrix} \succeq 0 \right\} \tag{14}$$

for some $Q_w \in \mathbb{R}^{N\times N}$, $S_w \in \mathbb{R}^{N\times m_d}$, $R_w \in \mathbb{R}^{m_d\times m_d}$ with $Q_w \prec 0$.

Remark 2: The form of the noise bound in Assumption 1 includes: the energy bound that $WW^{\mathrm{T}} = \sum_{i=1}^{N} w(i)w^{\mathrm{T}}(i) \preceq R_w$ by setting $Q_w = -I$, $S_w = 0$; the individual noise bound that $\|w(k)\| \le w_b$ which implies that $WW^{\mathrm{T}} = \sum_{i=1}^{N} w(i)w^{\mathrm{T}}(i) \preceq w_b^2 NI$ by setting $Q_w = -I$, $S_w = 0$, and $R_w = w_b^2 NI$ for $w_b > 0$. Other forms such as the sample covariance bound and the bounded noise within a subspace see [36].

Therefore, we define the set of system parameters that depends on the measured values with the noise satisfying Assumption 1 as

$$\Sigma_s := \left\{ (A\ B) \mid X_+ = AX + BU + B_w W, W \in \mathcal{W} \right\}. \tag{15}$$

By substituting (13) to the QMI in (14), we establish an equivalent formulation for Σ_s as follows.

Lemma 1: The set Σ_s in (15) is equal to

$$\Sigma_s = \left\{ [A\ B] \middle| \begin{bmatrix} [A\ B]^{\mathrm{T}}\\ I\end{bmatrix}^{\mathrm{T}} \Theta_s \begin{bmatrix} [A\ B]^{\mathrm{T}}\\ I\end{bmatrix} \succeq 0 \right\} \tag{16}$$

where

$$\Theta_s = \begin{bmatrix} Q_s & S_s\\ S_s^{\mathrm{T}} & R_s\end{bmatrix} := \begin{bmatrix} -\mathcal{Z} & 0\\ X_+ & B_w\end{bmatrix} \begin{bmatrix} Q_w & S_w\\ S_w^{\mathrm{T}} & R_w\end{bmatrix} \begin{bmatrix} -\mathcal{Z} & 0\\ X_+ & B_w\end{bmatrix}^{\mathrm{T}} \tag{17}$$

with $\mathcal{Z} := \mathrm{col}\{X, U\}$.

By using the data matrices X_+, X, U, and the bounded noise matrix W, a data-based representation characterized by a QMI is provided through Lemma 1. The set Σ_s contains all the systems explaining the noisy data, as well as the true system (1).

Remark 3: In the case of nonlinear systems control, a general way is identifying a linear system model at a nominal operation point to design the controller for a certain range of the operation point. This idea also applies to the proposed data-driven method. Assume that the values at the nominal operation point are x_{op} and u_{op}. Then the used measurements of the system trajectories are modified to $\{x(i) - x_{op}\}_{i=k_0}^{k_0+N}$ and $\{u(i) - u_{op}\}_{i=k_0}^{k_0+N-1}$.

III. Main Results

In this section, we first analyze the asymptotic stability of the augmented closed-loop system (10) without external disturbances by means of the aforementioned data-based representations. Subsequently, the data-based method for designing ZSET controller gains is proposed. In addition, a data-based design method for the H_∞ tracking controller is introduced to ensure that the closed-loop system (12) satisfies the H_∞ performance (11). Following that, a particular controller structure for dc–dc converters is presented in the context of dc microgrids. For symbol simplicity, we define

$$\varphi_{12} := \begin{bmatrix} I_n & 0_{n\times p} \\ 0_{m\times n} & 0_{m\times p} \end{bmatrix}, \ \varphi_{13} := \begin{bmatrix} 0_{n\times m} \\ I_m \end{bmatrix},$$
$$\varphi_{21} := \begin{bmatrix} I_n & 0_{n\times p} \\ 0_{p\times n} & I_p \end{bmatrix}, \ \varphi_{22} := \begin{bmatrix} 0_n & 0_{n\times p} \\ C & I_p \end{bmatrix}.$$

A. Data-Based Asymptotic Stability Analysis

Through Lemma 1 with the noisy data $\{x(i)\}_{i=k_0}^{k_0+N}$ and $\{u(i)\}_{i=k_0}^{k_0+N-1}$, data-based asymptotic stability conditions are derived on the basis of Lyapunov function technique.

Theorem 1: For a given matrix $\bar{K}$, the system (10) is asymptotically stable, if there exist $P \succ 0$ and $\lambda > 0$ with appropriate dimensions such that

$$\begin{bmatrix} -\varphi_{12}P\varphi_{12}^{\mathrm{T}} - \mathrm{sym}\{\varphi_{13}\bar{K}P\varphi_{12}^{\mathrm{T}}\} & \star & \star \\ -\varphi_{22}P\varphi_{12}^{\mathrm{T}} - \varphi_{22}P\bar{K}^{\mathrm{T}}\varphi_{13}^{\mathrm{T}} & \varphi_{21}P\varphi_{21}^{\mathrm{T}} - \varphi_{22}P\varphi_{22}^{\mathrm{T}} & \star \\ P\bar{K}^{\mathrm{T}}\varphi_{13}^{\mathrm{T}} & 0 & P \end{bmatrix} - \lambda \begin{bmatrix} I & 0 & 0 \\ 0 & [I\ 0] & 0 \end{bmatrix}^{\mathrm{T}} \Theta_s \begin{bmatrix} I & 0 & 0 \\ 0 & [I\ 0] & 0 \end{bmatrix} \succ 0 \tag{18}$$

holds, where Θ_s is defined as (17).

Proof: We construct the Lyapunov function for system (10) that $V(k) = \xi^{\mathrm{T}}(k)\bar{P}\xi(k)$, where $\bar{P} \succ 0$. The difference equation is obtained by direct calculation that

$$V(k+1) - V(k) = \xi^{\mathrm{T}}(k)((\bar{A}+\bar{B}\bar{K})^{\mathrm{T}}\bar{P}(\bar{A}+\bar{B}\bar{K}) - \bar{P})\xi(k). \tag{19}$$

Then, system (10) is asymptotically stable in the sense of Lyapunov if $(\bar{A}+\bar{B}\bar{K})^{\mathrm{T}}\bar{P}(\bar{A}+\bar{B}\bar{K}) - \bar{P} \prec 0$, which is dependent on model parameters $(A\ B)$ of system (1). Define that $P = \bar{P}^{-1}$ and then the model-based condition is equivalent to

$$P - (\bar{A}+\bar{B}\bar{K})P(\bar{A}+\bar{B}\bar{K})^{\mathrm{T}} \succ 0 \tag{20}$$

which can be rewritten as a QMI

$$\begin{bmatrix} I \\ \bar{A}^{\mathrm{T}} \\ \bar{B}^{\mathrm{T}} \end{bmatrix}^{\mathrm{T}} \begin{bmatrix} P & 0 & 0 \\ 0 & -P & -P\bar{K}^{\mathrm{T}} \\ 0 & -\bar{K}P & -\bar{K}P\bar{K}^{\mathrm{T}} \end{bmatrix} \begin{bmatrix} I \\ \bar{A}^{\mathrm{T}} \\ \bar{B}^{\mathrm{T}} \end{bmatrix} \succ 0. \tag{21}$$

By means of a Schur complement argument with $P \succ 0$ and matrix decomposition, the condition (18) is equivalent to

$$\begin{bmatrix} 0_{(n+m)\times(n+p)} & \varphi_{12} & \varphi_{13} \\ \varphi_{21} & \varphi_{22} & 0_{(n+p)\times m} \end{bmatrix} \begin{bmatrix} P & 0 & 0 \\ 0 & -P & -P\bar{K}^{\mathrm{T}} \\ 0 & -\bar{K}P & -\bar{K}P\bar{K}^{\mathrm{T}} \end{bmatrix} \begin{bmatrix} \star \end{bmatrix}^{\mathrm{T}} - \lambda \begin{bmatrix} I & 0 \\ 0 & [I\ 0] \end{bmatrix}^{\mathrm{T}} \Theta_s \begin{bmatrix} I & 0 \\ 0 & [I\ 0] \end{bmatrix} \succ 0. \tag{22}$$

Then by the full-block S-procedure [12] with the QMI in (16), the LMI (22) implies that

$$\begin{bmatrix} I & \\ \begin{bmatrix} I & 0 \\ 0 & 0 \\ 0 & I \end{bmatrix} \begin{bmatrix} A\ B \end{bmatrix}^{\mathrm{T}} \begin{bmatrix} I\ 0 \end{bmatrix} + \begin{bmatrix} 0 & C^{\mathrm{T}} \\ 0 & I \\ 0 & 0 \end{bmatrix} \end{bmatrix}^{\mathrm{T}} \begin{bmatrix} P & 0 & 0 \\ 0 & -P & -P\bar{K}^{\mathrm{T}} \\ 0 & -\bar{K}P & -\bar{K}P\bar{K}^{\mathrm{T}} \end{bmatrix} \begin{bmatrix} \star \end{bmatrix} \succ 0 \tag{23}$$

which is equivalent to (21). Hence, system (10) is asymptotically stable. ■

Remark 4: It can be seen that the stability condition in Theorem 1 is presented without any model knowledge, which is treated as uncertainty in the processing of linear fractional transformation (LFT). Compared with other QMI-based data-driven methods [11], [13], [14], [15], [17], [18], [19], the main challenge in the derivation of Theorem 1 is that the model parameters of the closed-loop system (10) is not corresponding to the elements of data-based representations (16), due to the introduction of the integrator state vector for tracking control.

B. Data-Based Zero Steady-State Error Tracking Controller Design

Based on Theorem 1, we propose a data-driven tracking control design method in what follows.

Theorem 2: The system (10) is asymptotically stable, if there exist $P \succ 0, \lambda > 0$ and L with appropriate dimensions such that

$$\begin{bmatrix} -\varphi_{12}P\varphi_{12}^{\mathrm{T}} - \mathrm{sym}\{\varphi_{13}L\varphi_{12}^{\mathrm{T}}\} & \star & \star \\ -\varphi_{22}P\varphi_{12}^{\mathrm{T}} - \varphi_{22}L^{\mathrm{T}}\varphi_{13}^{\mathrm{T}} & \varphi_{21}P\varphi_{21}^{\mathrm{T}} - \varphi_{22}P\varphi_{22}^{\mathrm{T}} & \star \\ L^{\mathrm{T}}\varphi_{13}^{\mathrm{T}} & 0 & P \end{bmatrix} - \lambda \begin{bmatrix} I & 0 & 0 \\ 0 & [I\ 0] & 0 \end{bmatrix}^{\mathrm{T}} \Theta_s \begin{bmatrix} I & 0 & 0 \\ 0 & [I\ 0] & 0 \end{bmatrix} \succ 0 \tag{24}$$

holds, where Θ_s is defined as (17). The tracking controller gain can be computed by $\bar{K} = LP^{-1}$.

Proof: In order to make $\bar{K}$ to be convex in the matrix inequality condition, the main change from Theorem 1 is the modification that $L = \bar{K}P$, i.e., the condition (24) implies (18). By solving the LMI (24), P and L are obtained and thus $\bar{K}$ can be calculated. Hence, system (10) is asymptotically stable. ■

Remark 5: There is an additional assumption for matrix Θ_s in derivations of controller design conditions in many QMI-based data-driven control methods such as [13], [14], [15], and [17]. However, it is not required in the presented work.

C. Data-Based H_∞ Tracking Controller Design

In view of external disturbances, we establish a data-driven H_∞ tracking control design method for system (12) thereinafter. For symbol simplicity, we define

$$\chi(k) := \mathrm{col}\{\xi(k), \bar{w}(k)\},$$
$$l_1 := [I_{m_d}, 0_{m_d\times(2n+3p)}],$$
$$l_2 := [0_{p\times m_d}, I_p, 0_{p\times(2n+2p)}],$$
$$l_3 := [0_{(n+p)\times(m_d+p)}, I_{n+p}, 0_{(n+p)\times(n+p)}],$$
$$l_4 := [0_{(n+p)\times(m_d+n+2p)}, I_{n+p}],$$
$$\Gamma_1 := \begin{bmatrix} I_n & 0_{n\times m} \\ 0_{p\times n} & 0_{p\times m} \\ 0_{m\times n} & I_m \end{bmatrix}, \Gamma_2 := \begin{bmatrix} 0_{n\times n} & C^{\mathrm{T}} \\ 0_{p\times n} & I_p \\ 0_{m\times n} & 0_{m\times p} \end{bmatrix}, \Gamma_3 := [I_n \ 0_{n\times p}].$$

Theorem 3: For a given scalar $\gamma > 0$, the closed-loop system (12) satisfies the H_∞ tracking performance (11), if there exist $P \succ 0$, $\lambda > 0$ and L with appropriate dimensions such that

$$\begin{bmatrix} \Gamma_1 & \Gamma_2 l_3 \\ 0 & I \end{bmatrix}^{\mathrm{T}} \begin{bmatrix} 0 & G^{\mathrm{T}} \\ G & \Psi \end{bmatrix} \begin{bmatrix} \Gamma_1 & \Gamma_2 l_3 \\ 0 & I \end{bmatrix} - \lambda \begin{bmatrix} I & 0 \\ 0 & \Gamma_3 l_3 \end{bmatrix}^{\mathrm{T}} \Theta_s \begin{bmatrix} I & 0 \\ 0 & \Gamma_3 l_3 \end{bmatrix} \succ 0 \tag{25}$$

holds, where

$$\Psi = l_1^{\mathrm{T}}(\gamma^2 I - \bar{B}_w^{\mathrm{T}}\bar{B}_w)l_1 + l_2^{\mathrm{T}}(I - \bar{C}P\bar{C}^{\mathrm{T}})l_2 + l_3^{\mathrm{T}}Pl_3 + l_4^{\mathrm{T}}Pl_4,$$
$$G = -l_2^{\mathrm{T}}\bar{C}[P^{\mathrm{T}}\ L^{\mathrm{T}}] + l_4^{\mathrm{T}}[P^{\mathrm{T}}\ L^{\mathrm{T}}]$$

with $\bar{C} = [C\ 0_{p\times p}]$, Θ_s is defined as (17). The tracking controller gain can be computed by $\bar{K} = LP^{-1}$.

Proof: We construct the Lyapunov function for system (12) that $V(k) = \xi^{\mathrm{T}}(k)\bar{P}\xi(k)$, where $\bar{P} \succ 0$. The difference equation is obtained by direct calculation that

$$\begin{aligned} &V(k+1) - V(k) \\ &= \xi^{\mathrm{T}}(k)((\bar{A}+\bar{B}\bar{K})^{\mathrm{T}}\bar{P}(\bar{A}+\bar{B}\bar{K}) - \bar{P})\xi(k) \\ &\quad + \bar{w}^{\mathrm{T}}(k)\bar{B}_w^{\mathrm{T}}\bar{B}_w\bar{w}(k) \\ &= \chi^{\mathrm{T}}(k)\Phi\chi(k) + \gamma^2\bar{w}^{\mathrm{T}}(k)\bar{w}(k) - \xi(k)^{\mathrm{T}}\bar{C}^{\mathrm{T}}\bar{C}\xi(k) \end{aligned} \tag{26}$$

where $\Phi = \begin{bmatrix} (\bar{A}+\bar{B}\bar{K})^{\mathrm{T}}\bar{P}(\bar{A}+\bar{B}\bar{K}) - \bar{P} + \bar{C}^{\mathrm{T}}\bar{C} & 0 \\ 0 & \bar{B}_w^{\mathrm{T}}\bar{B}_w - \gamma^2 I \end{bmatrix}$.

By the full-block S-procedure with the QMI in (16), the LMI (25) implies that

$$\begin{bmatrix} (\Gamma_1[A\ B]^{\mathrm{T}}\Gamma_3 + \Gamma_2)\ l_3 \\ I \end{bmatrix}^{\mathrm{T}} \begin{bmatrix} 0 & G^{\mathrm{T}} \\ G & \Psi \end{bmatrix} \begin{bmatrix} \star \end{bmatrix} \succ 0. \tag{27}$$

The left-hand side of the inequality (27) is equal to $\Psi + \mathrm{sym}\{-l_3^{\mathrm{T}}(\bar{A}+\bar{B}\bar{K})P\bar{C}^{\mathrm{T}}l_2 + l_3^{\mathrm{T}}(\bar{A}+\bar{B}\bar{K})Pl_4\}$. It can be illustrated in matrix form that

$$\begin{bmatrix} \gamma^2 I - \bar{B}_w^{\mathrm{T}}\bar{B}_w & 0 & 0 & 0 \\ 0 & I - \bar{C}P\bar{C}^{\mathrm{T}} & -\bar{C}P(\bar{A}+\bar{B}\bar{K})^{\mathrm{T}} & 0 \\ 0 & -(\bar{A}+\bar{B}\bar{K})P\bar{C}^{\mathrm{T}} & P & (\bar{A}+\bar{B}\bar{K})P \\ 0 & 0 & P^{\mathrm{T}}(\bar{A}+\bar{B}\bar{K})^{\mathrm{T}} & P \end{bmatrix}. \tag{28}$$

Define $P = \bar{P}^{-1}$. Through matrix decomposition and invoking Schur complement argument twice with $P \succ 0$, the condition that (28) is positive definite is equivalent to

$$\begin{bmatrix} \bar{P} & 0 & \bar{C}^{\mathrm{T}} & (\bar{A}+\bar{B}\bar{K})^{\mathrm{T}} \\ 0 & \gamma^2 I - \bar{B}_w^{\mathrm{T}}\bar{B}_w & 0 & 0 \\ \bar{C} & 0 & I & 0 \\ \bar{A}+\bar{B}\bar{K} & 0 & 0 & \bar{P}^{-1} \end{bmatrix} \succ 0. \tag{29}$$

It is easy to conclude that $\Phi \prec 0$. Then, we can obtain from (26) that $V(k+1) - V(k) \le \gamma^2\|\bar{w}(k)\|^2 - \|y(k) - r(k)\|^2$. Thus, we have $\sum_{k=k_0}^{Z}(V(k+1) - V(k)) \le \sum_{k=k_0}^{Z}(\gamma^2\|\bar{w}(k)\|^2 - \|y(k) - r(k)\|^2)$, i.e.,

$$V(Z+1) - V(k_0) \le \gamma^2 \sum_{k=k_0}^{Z} \|\bar{w}(k)\|^2 - \sum_{k=k_0}^{Z} \|y(k) - r(k)\|^2. \tag{30}$$

Under the zero initial condition $V(k_0) = 0$ and $V(k) > 0$ for $\chi \neq 0$, one has $\sum_{k=k_0}^{\infty}\|y(k) - r(k)\|^2 \le \gamma^2\sum_{k=k_0}^{\infty}\|\bar{w}(k)\|^2$ for $Z \to \infty$. Hence, the system (12) achieves the H_∞ tracking performance (11). ■

Remark 6: In the framework of QMI-based data-driven methods, QMIs are used to represent various bounds for noise samples and further represent the system matrices $(A\ B)$ through input-state data. By converting the results of model-based conditions to QMIs related to matrix variables $(A\ B)$, the purely data-driven conditions are obtained by the full-block S-procedure, as shown in the proof of Theorem 1. Thus, the ideas of Theorems 1, 2, and 3 can be extended to other existing model-based results for LTI systems.

D. Data-Driven Control for DC–DC Converters in DC Microgrids

On the basis of the aforementioned theories, we are about to design a data-driven control strategy for dc–dc converters. Notice that the considered controllers are the primary controllers in the hierarchical control framework, rather than the secondary controllers that modulate the steady-state objectives of the dc microgrid. The voltage of the capacitor and the current of the inductor are chosen as state variables of the dc–dc converter model with n_v capacitors and n_i inductors, i.e., $x(k) = \mathrm{col}\{v_c(k), i_L(k)\}$, where $v_c(k) \in \mathbb{R}^{n_v}$, $i_L(k) \in \mathbb{R}^{n_i}$ with $n_v + n_i = n$. The input $u(k)$ is the duty cycle. The state-averaging models of dc–dc converters are nonlinear, represented as

$$x(k+1) = f(x(k), u(k)). \tag{31}$$

However, in practice, the control strategies for dc–dc converters are generally applied along the nominal operation, which is determined in the design stage. Therefore, the dynamic of the nonlinear model (31) for a certain range of the operation point can be described by the LTI system (5). Define $v_c(k) = \mathrm{col}\{v_c^1(k), \ldots, v_c^{n_v-1}(k), v_o(k)\}$ and $i_L(k) = \mathrm{col}\{i_L^1(k), \ldots, i_L^{n_i}(k)\}$, where $v_o(k)$ is the voltage of the output filter capacitor. Given the output voltage of the dc–dc converter

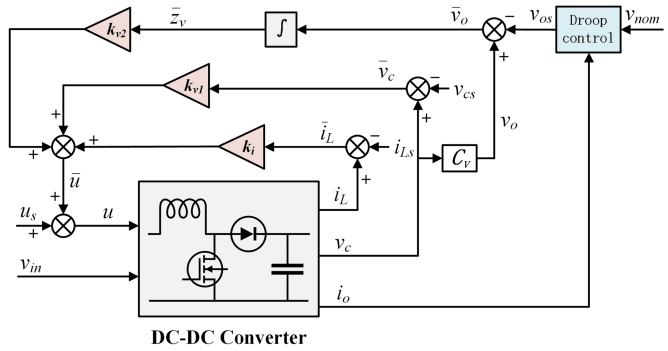

Fig. 1. Block diagram of the single-loop tracking controller.

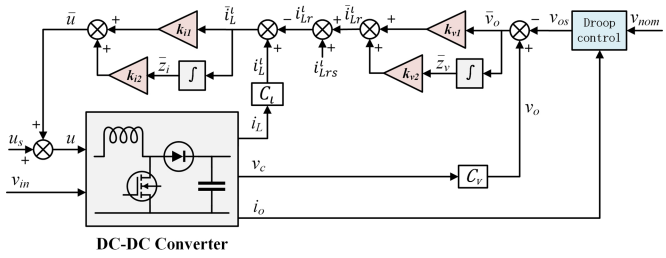

Fig. 2. Block diagram of the dual-loop tracking controller.

is equal to the voltage of the output filter capacitor, the output matrix of system (5) can be described as $C = [C_v, 0_{n_i}] = [0_{1\times(n_v-1)}, 1, 0_{1\times n_i}]$. As defined in Section II-A, the steady-state values are accordingly $x_s = \text{col}\{v_{cs}, i_{Ls}\}$ and u_s, where $v_{cs} = \text{col}\{v_{cs}^1, \ldots, v_{cs}^{n_v-1}, v_{os}\}$ and $i_{Ls} = \text{col}\{i_{Ls}^1, \ldots, i_{Ls}^{n_i}\}$. Note that v_{cs} and i_{Ls} are rating values, which are preset during the design stage of a dc microgrid. As state variables of the dc–dc converter model, the capacitor voltage and the inductor current are both imported into the feedback loops of the control system. Further considering that the goal is to regulate the output voltage $v_o(k)$ of the dc–dc converter to the set-point v_{os}, we construct an integrator state vector $z(k)$ for $v_o(k)$, and import it into the feedback loop to eliminate steady-state tracking errors. Therefore, the single-loop dynamic feedback controller can be designed as

$$\bar{u}(k) = k_{v1}\bar{v}_c(k) + k_{v2}\bar{z}_v(k) + k_i\bar{i}_L(k) \tag{32}$$

where $\bar{u}(k) = u(k) - u_s$, $\bar{v}_c(k) = v_c(k) - v_{cs} = \text{col}\{\bar{v}_c^1(k), \ldots, \bar{v}_c^{n_v-1}(k), \bar{v}_o(k)\}$, $\bar{i}_L(k) = i_L(k) - i_{Ls} = \text{col}\{\bar{i}_L^1(k), \ldots, \bar{i}_L^{n_i}(k)\}$. The integrator state vector of $v_o(k)$ satisfies $\bar{z}_v(k+1) = \bar{z}_v(k) + \bar{v}_o(k)$. That is, the controller gains in (6) is represented as $K_1 = [k_{v1},\ k_i]$, $K_2 = k_{v2}$. The controller structure is depicted in Fig. 1.

Furthermore, the dual-loop controller composed of an inner current loop and an outer voltage loop can be described as

$$\begin{aligned}\bar{u}(k) &= k_{i1}\bar{i}_L^\iota(k) + k_{i2}\bar{z}_i(k),\\ \bar{i}_{Lr}^\iota(k) &= k_{v1}\bar{v}_o(k) + k_{v2}\bar{z}_v(k)\end{aligned} \tag{33}$$

where $\bar{i}_L^\iota(k)$ is the error between the sampled signal $i_L^\iota(k)$ and its reference signal $i_{Lr}^\iota(k)$. $i_L^\iota(k) = C_\iota i_L(k)$ is the ιth inductor current of $i_L(k)$ to be controlled, i.e. $C_\iota = [0_{1\times(\iota-1)}, 1, 0_{1\times(n_i-\iota)}]$. The integrator state vector of $i_L^\iota(k)$ satisfies $\bar{z}_i(k+1) = \bar{z}_i(k) + \bar{i}_L^\iota(k)$. The reference signal $i_{Lr}^\iota(k)$ of the inner current loop is the sum of a given rating value i_{Lrs}^ι and the output of the voltage loop, i.e., $i_{Lr}^\iota(k) = i_{Lrs}^\iota + \bar{i}_{Lr}^\iota(k)$. The dual-loop controller structure is depicted in Fig. 2. The gains of the inner current loop controller in (6) are represented as $K_1 = k_{i1}$, $K_2 = k_{i2}$, and the output matrix of the linearized system (5) is $C = 1$, i,e, $\bar{y}(k) = \bar{x}(k) = \bar{i}_L^\iota(k)$. Regarding the linearized system of the dc–dc converter interconnected with the designed inner loop controller, the gains of the outer voltage loop controller are represented as $K_1 = k_{v1}$, $K_2 = k_{v2}$, and the output matrix is $C = 1$, i,e, $\bar{y}(k) = \bar{x}(k) = \bar{v}_o(k)$.

Algorithm 1: Data-driven Zero Steady-state Error Tracking Control Algorithm for a DC–DC Converter

Step 1. Perform an open-loop experiment with an exciting signal around the operation point of the DC–DC converter.

Step 2. Sample the input and state data of system trajectories $\{u(i)\}_{i=k_0}^{k_0+N-1}$ and $\{x(i)\}_{i=k_0}^{k_0+N}$ from the moment k_0.

Step 3. Calculate the difference between the sampled signals and the steady-state values, i.e. $\{u(i) - u_s\}_{i=k_0}^{k_0+N-1}$ and $\{x(i) - x_s\}_{i=k_0}^{k_0+N}$.

Step 4. With the data obtained in *Step 3*, solve the LMI (24) to obtain P and L.

Step 5. Compute the controller gain $\bar{K} = LP^{-1}$.

To achieve data-driven control, the data of the system trajectories $\{x(i)\}_{i=k_0}^{k_0+N}$ and $\{u(i)\}_{i=k_0}^{k_0+N-1}$, $k_0 \in \mathbb{N}_0$, $N \in \mathbb{N}_+$ are measured, by applying an open-loop excitation around the operation point u_s. As mentioned in Remark 3, the data used for control design are the difference between the sampled signals and the steady-state values, i.e. $\{x(i) - x_s\}_{i=k_0}^{k_0+N}$ and $\{u(i) - u_s\}_{i=k_0}^{k_0+N-1}$. For the single-loop controller, the data-driven ZSET control algorithm and the data-driven H_∞ tracking control algorithm for a dc–dc converter can be summarized as Algorithms 1 and 2, respectively. For the latter, the minimum estimated value of γ can be obtained via a bisection algorithm, i.e. *Steps 4–6* in Algorithm 2. For the dual-loop controller, the data-driven control algorithm can be described as Algorithm 3, where the data collection process and the controller gain calculation based on Theorem 2 follow the order of inner loop first and then outer loop. In a similar way, Theorem 3 can also be utilized in Algorithm 3 to compute controller gains.

In the case of multiple dc–dc converters supplied in parallel, the controller design for parallel-connected dc–dc converters can be dealt with in an incremental process. That is, for the new converter connected to the dc microgrid that already contains the converters equipped with the designed controllers, the control algorithm is performed similarly. By interconnecting in open-loop to the dc-bus of the closed-loop converters, the dynamic of the newly added converter captured by the measured data contains the interconnections of other converters and loads.

Algorithm 2: Data-driven H_∞ Tracking Control Algorithm for a DC–DC Converter

Step 1. Perform an open-loop experiment with an exciting signal around the operation point of the DC–DC converter.
Step 2. Sample the input and state data of system trajectories $\{u(i)\}_{i=k_0}^{k_0+N-1}$ and $\{x(i)\}_{i=k_0}^{k_0+N}$ from the moment k_0.
Step 3. Calculate the difference between the sampled signals and the steady-state values, i.e. $\{u(i)-u_s\}_{i=k_0}^{k_0+N-1}$ and $\{x(i)-x_s\}_{i=k_0}^{k_0+N}$.
Step 4. Set an initial estimated upper value of H_∞ performance index $\gamma_u > 0$, which is required to be feasible for solving the LMI (25). Set an initial estimated lower value of H_∞ performance index $\gamma_l > 0$, which is required to be infeasible for solving the LMI (25).
Step 5. For the given γ_u and γ_l, compute $\gamma_m = (\gamma_u + \gamma_l)/2$. If the LMI (25) is feasible for γ_m, set $\gamma_u = \gamma_m$; otherwise set $\gamma_l = \gamma_m$.
Step 6. For the preset goal error e_γ, if $|\gamma_u - \gamma_m| > e_\gamma$, go to *Step 5*; otherwise go to *Step 7*.
Step 7. For the given γ_u in *Step 6*, set $\gamma = \gamma_u$ and solve the LMI (25) to obtain P and L.
Step 8. Compute the controller gain $\bar{K} = LP^{-1}$.

Remark 7: In terms of algorithm complexity, the time taken to solve the LMI in the algorithm is very short (CPU time is less than 0.5 s). Moreover, the control design for converters is during the design stage of the original or upgraded dc microgrids. Thus, the algorithms do not need to be executed in real time.

Remark 8: In order to achieve power sharing of parallel-connected dc–dc converters, the droop control [25] can be utilized, as presented in Fig. 1. The reference of the output voltage v_{os} is determined by $v_{os} = v_{nom} - k_d i_o$, where v_{nom} is the nominal voltage, i_o is the measurable output current, and k_d is the droop gain.

IV. Experimental Results

In this section, the proposed data-driven control design methods are validated by simulations and experiments. In Section IV-A, a single ended primary inductor converter (SEPIC) is firstly considered to verify the designed single-loop voltage control strategy of the dc–dc converter in simulations. Then, we consider a dc microgrid with parallel-connected dc–dc converters, i.e. the interconnection of a boost converter, a buck converter, and loads, where voltage regulation and power sharing are both implemented. In Section IV-B, the experiment investigation is conducted based on the hardware prototype including the power circuitry to verify both the single-loop control algorithm and the dual-loop control algorithm.

A. Simulation Examples

1) Control of Single SEPIC
The SEPIC is used in numerous applications such as the solar power generation field [37]. The structure of the SEPIC is shown in Fig. 3. The parameters of the SEPIC are $L_1 = L_2 = 150\ \mu$H, $C_1 = 47\ \mu$F, and $C_2 = 250\ \mu$F. The load resistance is $R_o = 10\ \Omega$. The input voltage is $v_{in} = 25$ V. The reference of the output voltage is $v_{os} = 50$ V. The switching frequency is $f_w = 50$ kHz. The control period of the proposed dynamic feedback tracking controllers is set to $T_{c1} = 0.01$ ms. The goal of the data-based controller is to regulate the output voltage v_o of the SEPIC to v_{os}. The power system simulation is based on SIMULINK. The controller gains are obtained by solving the LMI through Yalmip with Mosek in MATLAB. The data-driven control design begins with the data acquisition during an open-loop experiment of the system. The steady-state value of the duty cycle is $u_s = v_{os}/(v_{in} + v_{os}) = 2/3$. Thus, the exciting signal is set to

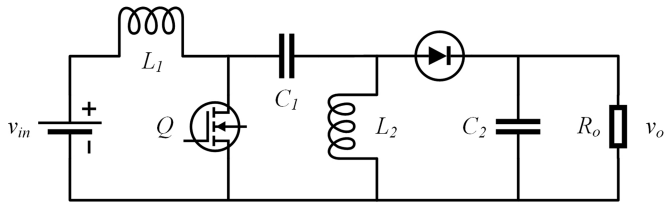

Fig. 3. Structure of the SEPIC.

Algorithm 3: Data-driven Dual-loop Tracking Control Algorithm for a DC–DC Converter

Step 1. For the inner current control, perform an open-loop experiment with an exciting signal around the operation point of the DC–DC converter.
Step 2. Sample the input (duty cycle) and state (the controlled inductor current) data of system trajectories $\{u(i)\}_{i=k_0}^{k_0+N-1}$ and $\{i_L^\iota(i)\}_{i=k_0}^{k_0+N}$ from the moment k_0.
Step 3. Calculate the difference between the sampled signals and the steady-state values, i.e. $\{u(i)-u_s\}_{i=k_0}^{k_0+N-1}$ and $\{i_L^\iota(i)-i_{Lr}^\iota\}_{i=k_0}^{k_0+N}$.
Step 4. With the data obtained in *Step 3*, solve the LMI (24) to obtain P and L.
Step 5. Compute the inner current loop controller gain $\bar{K} = LP^{-1}$.
Step 6. For the outer voltage control, perform an open-loop experiment with an exciting signal around the operation point of the DC–DC converter interconnected with the inner loop controller designed in *Step 5*.
Step 7. Sample the input (reference of the controlled inductor current) and state (output voltage) data of system trajectories $\{i_{Lr}^\iota(i)\}_{i=k_0}^{k_0+N-1}$ and $\{v_o(i)\}_{i=k_0}^{k_0+N}$ from the moment k_0.
Step 8. Calculate the difference between the sampled signals and the steady-state values, i.e. $\{i_{Lr}^\iota(i)-i_{Lrs}^\iota\}_{i=k_0}^{k_0+N-1}$ and $\{v_o(i)-v_{os}\}_{i=k_0}^{k_0+N}$.
Step 9. With the data obtained in *Step 8*, solve the LMI (24) to obtain P and L.
Step 10. Compute the outer voltage loop controller gain $\bar{K} = LP^{-1}$.

$u(k) = 0.01\sin(0.01\pi k) + 2/3$. The noise sequence W is sampled uniformly from $[-w_b, w_b]$, where $w_b = 0.005$. Through Assumption 1, the noise $w(k)$ is individually bounded in Euclidean norm by w_b, by setting $Q_w = -I$, $S_w = 0$, and $R_w = w_b^2 NI$.

The state x consists of the voltage v_c^1, v_o, and the current i_L^1, i_L^2, where the voltage of the capacitor C_2 is equal to the output voltage v_o. By sampling input data $U = [u(0), u(1), \ldots, u(N-1)]$, we can obtain state sequences $X = [x(0), x(1), \ldots, x(N-1)]$ and $X_+ = [x(1), x(2), \ldots, x(N)]$ accordingly, where $N = 1000$. Then we calculate the difference sequences respectively that $\{u(i) - u_s\}_{i=0}^{N-1}$, $\{x(i) - x_s\}_{i=0}^{N-1}$, and $\{x(i) - x_s\}_{i=1}^{N}$. By solving LMI (24) with the calculated data, we can compute the ZSET controller gains

$$\bar{K} = [0.00024, -0.0237, -0.00662, -0.00811, -0.876].$$

Based on the form of the dynamic feedback controller (32), the computed gains of the controller correspond to $\bar{v}_c^1$, $\bar{v}_o$, $\bar{i}_L^1$, $\bar{i}_L^2$ and the integrator state vector of $\bar{v}_o$ in sequence.

Similarly, through LMI (25) with the calculated data, we can obtain the H_∞ tracking controller gains

$$\bar{K} = [-0.00017, -0.0593, -0.0124, -0.0011, -0.962].$$

The proposed data-driven dynamic feedback controller designing methods are compared with the data-based stabilization control design method in [11] and the DeePC method in [9]. The data-based stabilization control method is similarly based on the system representation from noisy data in the form of QMI, without considering the integrator state vector. The control period is the same as the dynamic feedback tracking controller, i.e. $T_{c1} = 0.01$ ms. Utilizing the LMI (FS) in [11] with the sampled noisy data mentioned above, the stabilization controller gains are computed as

$$\bar{K} = [0.0016, -0.0031, -0.0004, -0.0028]$$

where the four proportional feedback gains correspond to $\bar{v}_c^1$, $\bar{v}_o$, $\bar{i}_L^1$ and $\bar{i}_L^2$ in sequence. For the DeePC method, where the traditional MPC optimization problem is formulated into a data-based form through the precollected data satisfying the persistence of the excitation condition [6], we choose $L = 30$ for the prediction horizon with the parameters $Q = \text{diag}\{1, 10^3, 1, 1\}$, $R = 1$. Since the single execution time of DeePC is around 10 to 20 ms, the control period is set to 20 ms to ensure that the algorithm works as expected.

To verify the robust performance of the data-driven controller, we impose the disturbance on input voltage within a range of ± 7V and change the load within a range of $\pm 20\%$, respectively. The results are shown in Figs. 4 and 5. It can be seen that the output voltage of the controlled SEPIC remains constant. The proposed data-based dynamic feedback controllers including the ZSET controller and the H_∞ tracking controller are superior in terms of the steady-state error. Moreover, with the robust performance constraint, the H_∞ tracking controller achieves a smaller overshoot than the ZSET controller in the case of load variation. In terms of the ZSET controller and the H_∞ tracking controller, considering similar dynamic behaviors of the closed-loop systems and the length constraints on the article content, the simulated and experimental results of the data-based H_∞ tracking controller are presented subsequently.

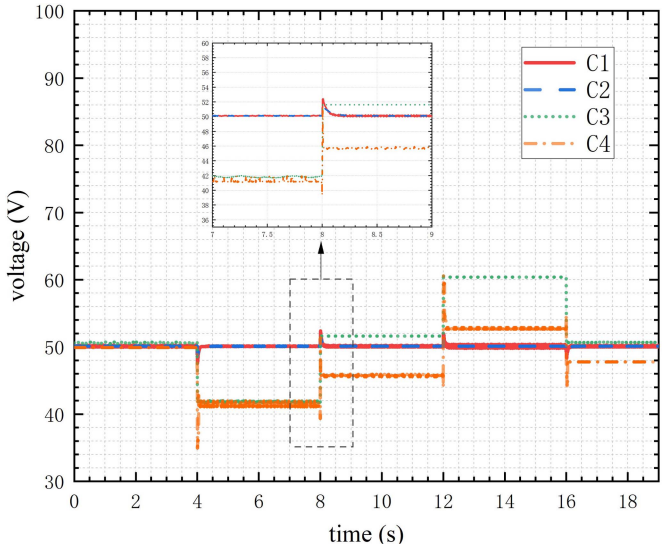

Fig. 4. Output voltage response with input voltage variation for the SEPIC. (C1: ZSET controller; C2: H_∞ tracking controller; C3: Stabilization controller; C4: DeePC.).

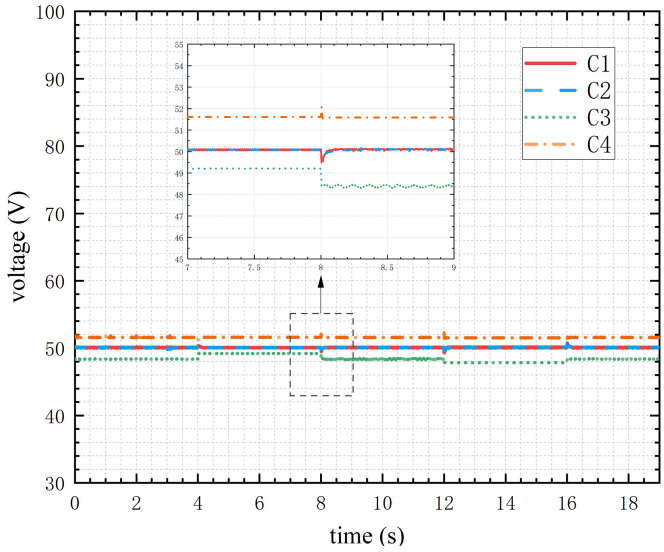

Fig. 5. Output voltage response with $\pm 20\%$ load variation for the SEPIC. (C1: ZSET controller; C2: H_∞ tracking controller; C3: Stabilization controller; C4: DeePC.).

2) Control of Parallel-Connected dc–dc Converters

The dc microgrid with parallel-connected dc–dc converters is depicted in Fig. 6. The parameters of the dc microgrid are input voltage of the boost converter, $v_{in1} = 50$ V; input voltage of the buck converter, $v_{in2} = 200$ V; the

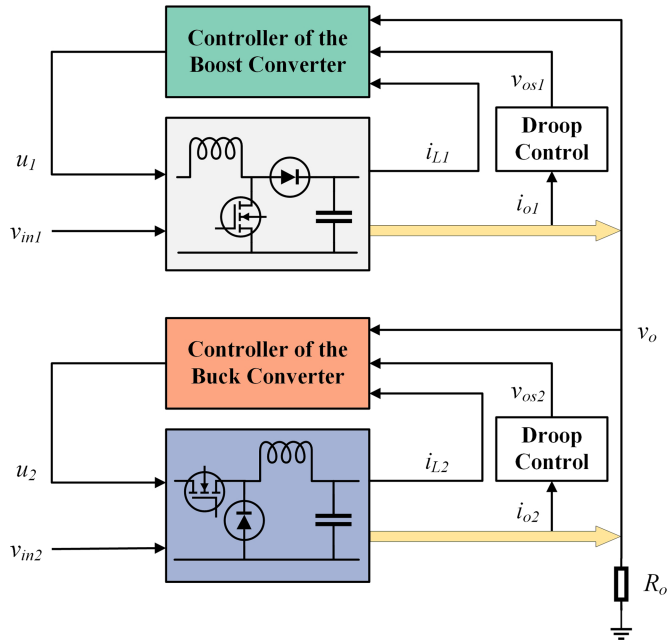

Fig. 6. DC microgrid including parallel-connected DC–DC converters.

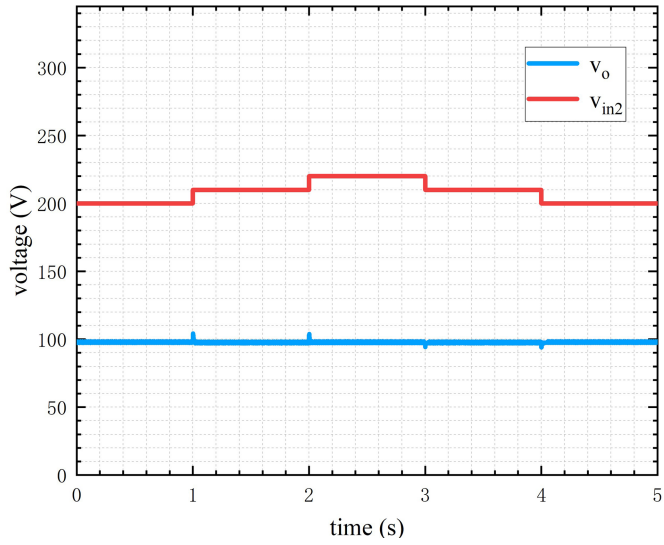

Fig. 7. Output voltage response with input voltage variation for parallel-connected DC–DC converters.

reference of the output voltage, i.e. dc-bus voltage, $v_{os} = 100$ V; load resistance, $R_o = 10\ \Omega$; switching frequency, $f_w = 50$ kHz; control period, $T_{c1} = 0.01$ ms. The parameters of the boost converter are $L_1 = 238\ \mu$H and $C_1 = 10\ \mu$F. The parameters of the buck converter are $L_2 = 328\ \mu$H and $C_2 = 96\ \mu$F. One of the goals of the data-based controllers is to regulate the output voltage v_o of the dc-bus to v_{os}. Another one is to achieve power sharing of parallel-connected dc–dc converters. For this purpose, the droop gains of the boost converter and the buck converter are $k_{d1} = 0.4$ and $k_{d2} = 0.6$, respectively. We first design the controller for the boost converter. In the open-loop experiment for data acquisition, the steady-state value of the duty cycle is $u_{1s} = 1 - v_{in1}/v_{os} = 0.5$. Thus, the exciting signal is set to $u(k) = 0.02\sin(0.008\pi k) + 0.5$. The noise sequence W is sampled uniformly from $[-w_b, w_b]$, where $w_b = 0.05$. Through Assumption 1, the noise $w(k)$ is individually bounded in Euclidean norm by w_b, by setting $Q_w = -I$, $S_w = 0$, and $R_w = w_b^2 NI$.

The state x consists of the voltage of the capacitor v_o, i.e. the output voltage, and the current of the inductor i_{L1} of the boost converter. By sampling input data U, we can obtain state sequences X and X_+ accordingly, where the number of samples is 1000. Then, we calculate the difference sequences, respectively, that $\{u(i) - u_{1s}\}_{i=0}^{N-1}$, $\{x(i) - x_s\}_{i=0}^{N-1}$, and $\{x(i) - x_s\}_{i=1}^{N}$. By solving LMI (25) with the calculated data, we have the H_∞ tracking controller gains

$$\bar{K} = [0.00312, -0.0129, -0.255]$$

where the computed gains of the controller correspond to $\bar{v}_o$, $\bar{i}_{L1}$ and the integrator state vector of $\bar{v}_o$ in sequence.

A buck converter is interconnected to the dc-bus of the boost converter, as depicted in Fig. 6. The goal is to design the controller for the new converter to regulate the voltage of the dc-bus and achieve power sharing of two converters. To this end, an open-loop experiment for the buck converter is conducted, which is similar to the boost converter. Note that the steady-state value of the duty cycle is $u_{2s} = v_{os}/v_{in2} = 0.5$ for the buck converter. Sample W uniformly from $[-w_b, w_b]$ and set $Q_w = -I$, $S_w = 0$, and $R_w = w_b^2 NI$, where $w_b = 0.05$. Then, we can obtain 1000 measurements of U, X, and X_+. The state x consists of the output voltage v_o and the current of the inductor i_{L2} of the buck converter. By calculating the difference sequences and solving LMI (25), we can compute the controller gains

$$\bar{K} = [0.00194, -0.0086, -0.223]$$

where the computed gains correspond to $\bar{v}_o$, $\bar{i}_{L2}$ and the integrator state vector of $\bar{v}_o$ in sequence.

We first impose the disturbance on the input voltage of the buck converter to verify the robust performance of the data-driven controller. As illustrated in Figs. 7 and 8, the voltage of the dc-bus and the current of the inductor are robustly stabilized by the designed controller. Then, we change the load within a range of $\pm 15\%$ to verify the power sharing capability. Figs. 9 and 10 imply that the currents are adjusted as expected, while the dc-bus voltage keeps stability.

The proposed control strategies are suitable for the modular dc microgrid [26]. Specifically, the controllers for power converters, which are designed in an incremental process during network capabilities upgrade, can achieve a satisfactory stability performance even after the distributed generation (DG) modules are inserted as well as removed in the order of module expansion. The considered DG includes a dc source, a dc–dc converter, and the local load [38]. To verify the ability of plug-and-play (PnP) functionality, we consider a DG v_{in1} including the aforementioned boost converter and a DG v_{in2} including the aforementioned buck converter, where the local loads of DG

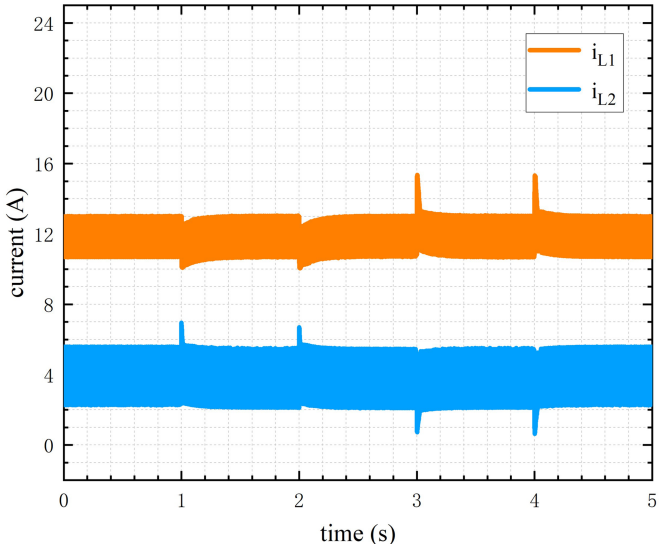

Fig. 8. Current response with input voltage variation for parallel-connected DC–DC converters.

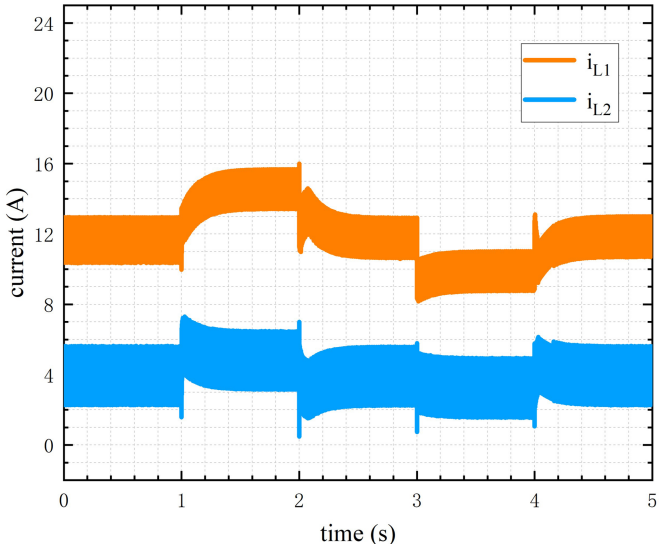

Fig. 10. Current response with ±15% load variation for parallel-connected DC–DC converters.

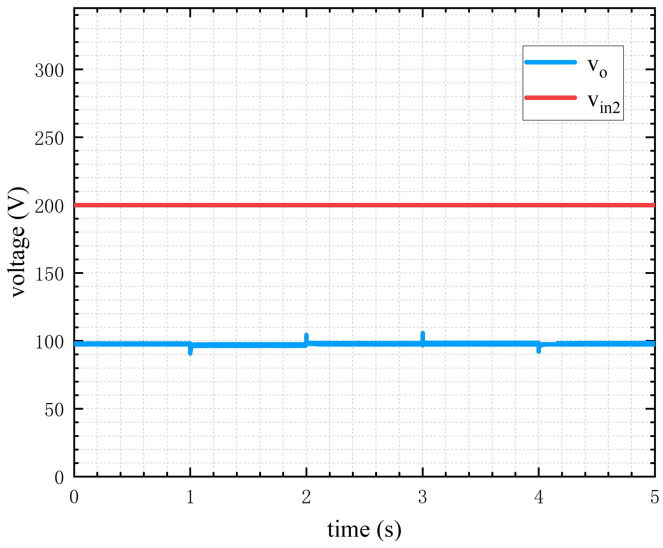

Fig. 9. Output voltage response with ±15% load variation for parallel-connected DC–DC converters.

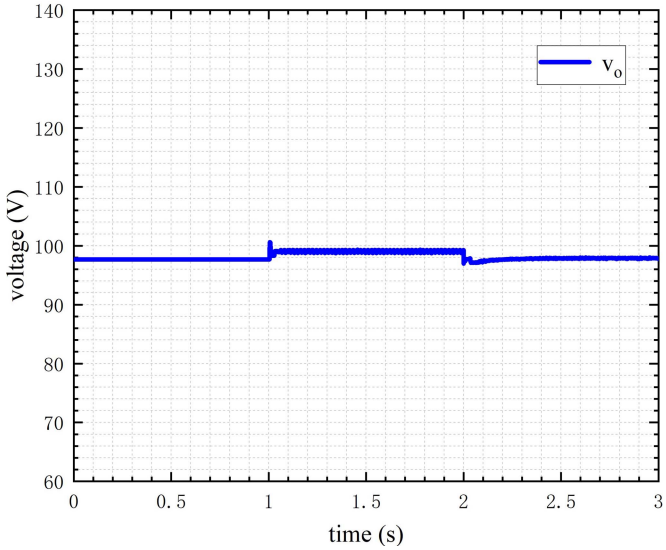

Fig. 11. Output voltage response of DG v_{in1} under plug-out of DG v_{in2} at $t = 1s$ and its plug-in at $t = 2$s.

v_{in1} and DG v_{in2} are both $R_L = 20\ \Omega$. Figs. 11 and 12 show the closed-loop performance during the plug in/out of the DG v_{in2} to/from the DG v_{in1}. It can be seen that the output voltage remains stable and the output currents are adjusted as expected even after incremental addition or removal of new devices.

B. Hardware Experiments

As depicted in Fig. 13, the hardware experiment platform consists of a dc–dc buck converter, a dc voltage source, the Rapid Control Prototype (RCP), the load module, and the upper computer display module. The parameters of the buck converter are $L = 1.6$ mH and $C = 4$ mF. The load resistance is $R_o = 20\ \Omega$. The input voltage is $v_{in} = 30$ V. The reference of the output voltage is $v_{os} = 10$ V. The switching frequency is $f_{wE} = 20$ kHz. The control period is set to $T_{c2} = 0.1$ ms. The goal is to design a data-based controller to regulate the output voltage v_o of the buck converter to v_{os}.

For the single-loop controller, since the steady-state value of the duty cycle is $u_s = v_{os}/v_{in} = 1/3$, the exciting signal is set to $u(k) = 0.05\sin(0.0133\pi k) + 1/3$ in the open-loop experiment. Sample W uniformly from $[-w_b, w_b]$ and set $Q_w = -I$, $S_w = 0$, and $R_w = w_b^2 NI$, where $w_b = 0.01$. Then we can obtain measurements that U, X, and X_+, where the number of samples is 1000. The state x consists of the output voltage v_o and the current of the inductor i_L. By means of LMI (25), we can compute the controller gains

$$\bar{K} = [-0.00811, -0.08784, -0.51503]$$

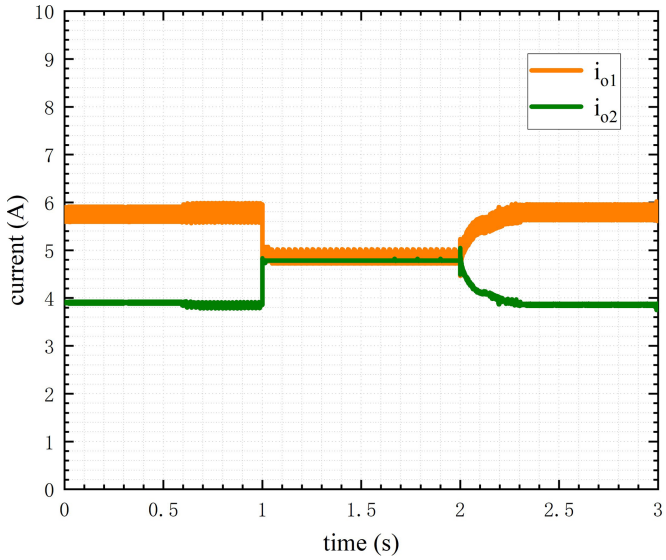

Fig. 12. Output current response under plug-out of DG v_{in2} at $t = 1s$ and its plug-in at $t = 2$s.

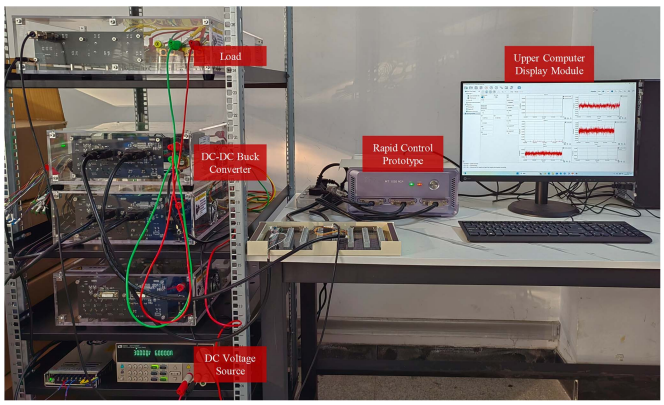

Fig. 13. Hardware experiment platform.

where the computed gains correspond to $\bar{v}_o, \bar{i}_L$ and the integrator state vector of $\bar{v}_o$ in sequence.

For the inner current loop of the dual-loop controller, the settings for the data collection are the same as the single-loop controller, where the sampled state is the inductor current rather than the output voltage. Through *Steps 1–5* in Algorithm 3, we can compute the controller gains of the inner current loop

$$\bar{K} = [-0.2073, -1.283]$$

where the computed gains correspond to $\bar{i}'_L$ and the integrator state vector of $\bar{i}'_L$ in sequence. As for the outer voltage loop, since the steady-state value of the inductor current reference, i.e., the rating value of the inductor current, is $i'_{Lrs} = 0.5$, the exciting signal is set to $i'_{Lr}(k) = 0.5\sin(0.00266\pi k) + 0.5$ in the open-loop experiment for the buck converter interconnected with the designed inner loop controller. Other settings for the data collection are the same as the single-loop controller. Through *Step 6-Step 10* in Algorithm 3, we can compute the controller

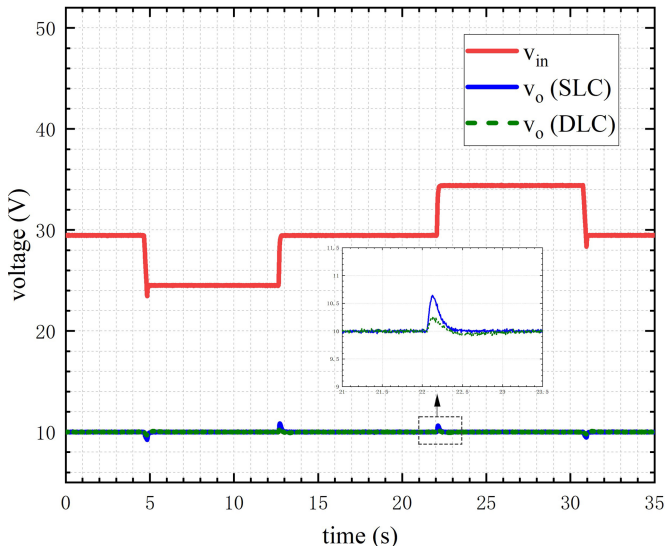

Fig. 14. Output voltage response with input voltage variation for the buck converter in hardware experiments.

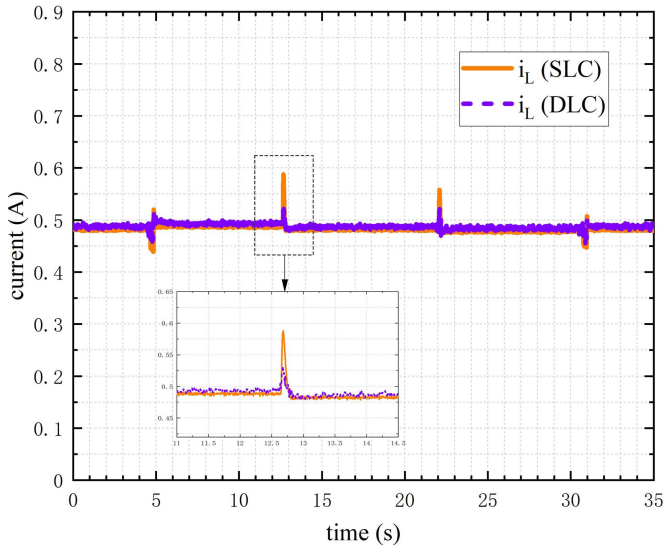

Fig. 15. Current response with input voltage variation for the buck converter in hardware experiments.

gains of the outer voltage loop

$$\bar{K} = [-0.4407, -2.058]$$

where the computed gains correspond to $\bar{v}_o$ and the integrator state vector of $\bar{v}_o$ in sequence.

As illustrated in Figs. 14 and 15, where SLC and DLC represent the single-loop controller and the dual-loop controller, respectively, the output voltage and the inductor current are robustly stabilized by the data-based controller with input voltage variation. The dual-loop controller achieves smaller output voltage overshoots and smaller current oscillations. In addition, Figs. 16 and 17 imply that the output voltage keeps stability and the current is adjusted as anticipated when the load is doubled at 5 s and then halved at 15 s, which verifies the

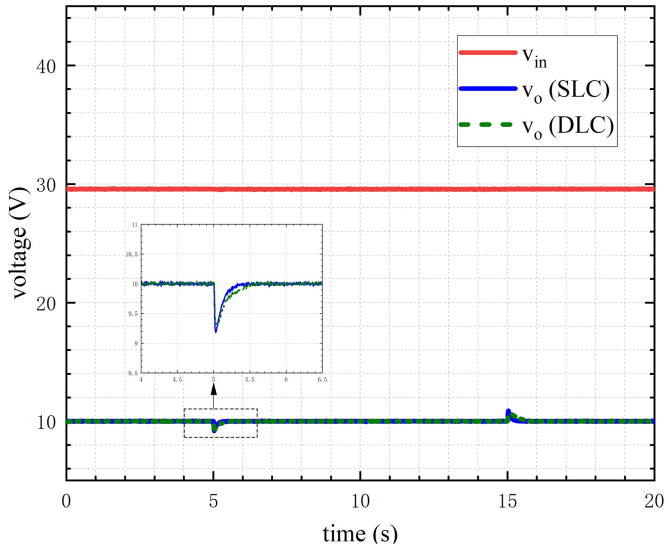

Fig. 16. Output voltage response with load variation for the buck converter in hardware experiments.

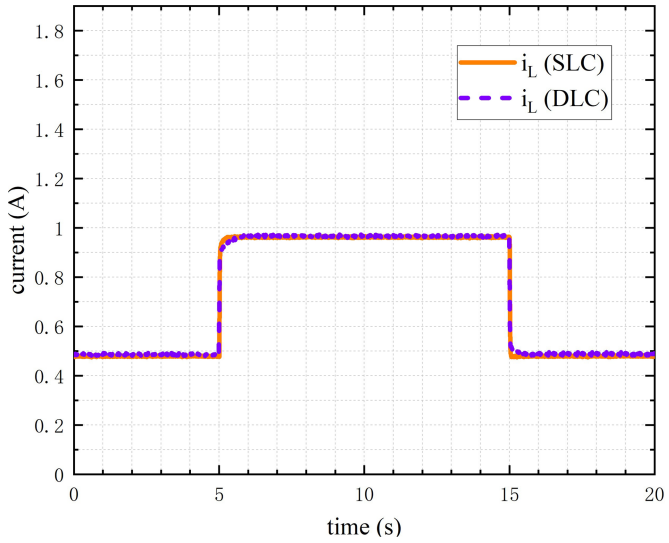

Fig. 17. Current response with load variation for the buck converter in hardware experiments.

effectiveness of both the single-loop controller and the dual-loop controller.

V. Conclusion

In this paper, we study data-driven analysis and control design for dc–dc converters in dc microgrids. Data-driven control algorithms for two dynamic feedback tracking controllers are proposed. Instead of identifying explicit systems, the control algorithms are achieved through measurements of system trajectories with rigorous theoretical derivations. The considered noise affects not only the measurement accuracy, but also the system dynamics, which is more suitable for practical applications. Note that the relationship between data-driven control and model-based control should be complementary rather than exclusive, based on their respective advantages and disadvantages. For instance, by virtue of its ability to extract system characteristics from actual field data, data-based results can be used to guide the optimization of control parameters initially tuned according to the model-based approach. For future work, PnP-oriented data-driven distributed control design for multibus dc microgrids may be an interesting topic. Moreover, the RCP-based controller can be replaced with a microcontroller unit to validate the data-driven control algorithms, which is closer to the mass production environment.

References

[1] C. De Persis and P. Tesi, "Formulas for data-driven control: Stabilization, optimality, and robustness," *IEEE Trans. Autom. Control*, vol. 65, no. 3, pp. 909–924, Mar. 2020.

[2] F. Dörfler, P. Tesi, and C. De Persis, "On the certainty-equivalence approach to direct data-driven LQR design," *IEEE Trans. Autom. Control*, vol. 68, no. 12, pp. 7989–7996, Dec. 2023.

[3] L. Ljung, *System Identification*. Cambridge, MA, USA: Birkhäuser, 1998.

[4] R. Zhao, W. Deng, Y. Wang, K. Huang, B. Zheng, and J. Ding, "An improved data-driven method for steering feedback torque of driving simulator," *IEEE/ASME Trans. Mechatron.*, vol. 28, no. 5, pp. 2953–2963, Oct. 2023.

[5] A. Nikolakopoulou, M. S. Hong, and R. D. Braatz, "Dynamic state feedback controller and observer design for dynamic artificial neural network models," *Automatica*, vol. 146, 2022, Art. no. 110622.

[6] J. C. Willems, P. Rapisarda, I. Markovsky, and B. L. De Moor, "A note on persistency of excitation," *Syst. Control Lett.*, vol. 54, no. 4, pp. 325–329, 2005.

[7] L. Xu, M. S. Turan, B. Guo, and G. Ferrari-Trecate, "Non-conservative design of robust tracking controllers based on input-output data," in *Proc. 3 rd Conf. Learn. Dyn. Control*, 2021, pp. 138–149.

[8] W. Liu, J. Sun, G. Wang, F. Bullo, and J. Chen, "Data-driven resilient predictive control under denial-of-service," *IEEE Trans. Autom. Control*, vol. 68, no. 8, pp. 4722–4737, Aug. 2023.

[9] J. Bongard, J. Berberich, J. Köhler, and F. Allgöwer, "Robust stability analysis of a simple data-driven model predictive control approach," *IEEE Trans. Autom. Control*, vol. 68, no. 5, pp. 2625–2637, May 2023.

[10] M. Rotulo, C. D. Persis, and P. Tesi, "Data-driven linear quadratic regulation via semidefinite programming," *IFAC-PapersOnLine*, vol. 53, no. 2, pp. 3995–4000, 2020.

[11] H. J. van Waarde, M. K. Camlibel, and M. Mesbahi, "From noisy data to feedback controllers: Nonconservative design via a matrix S-lemma," *IEEE Trans. Autom. Control*, vol. 67, no. 1, pp. 162–175, Jan. 2022.

[12] C. W. Scherer, "LPV control and full block multipliers," *Automatica*, vol. 37, no. 3, pp. 361–375, 2001.

[13] S. Wildhagen, J. Berberich, M. Hirche, and F. Allgöwer, "Improved stability conditions for systems under aperiodic sampling: Model- and data-based analysis," in *Proc. IEEE 60th Conf. Decis. Control*, 2021, pp. 5795–5801.

[14] J. Berberich, S. Wildhagen, M. Hertneck, and F. Allgöwer, "Data-driven analysis and control of continuous-time systems under aperiodic sampling," *IFAC-PapersOnLine*, vol. 54, no. 7, pp. 210–215, 2021.

[15] J. Berberich, C. W. Scherer, and F. Allgöwer, "Combining prior knowledge and data for robust controller design," *IEEE Trans. Autom. Control*, vol. 68, no. 8, pp. 4618–4633, Aug. 2023.

[16] W.-L. Qi, K.-Z. Liu, R. Wang, and C.-Y. Xu, "Data-driven tracking control for uncertain linear systems using a dual-system approach," *IEEE Control Syst. Lett.*, vol. 7, pp. 3331–3336, Jul. 2023.

[17] X. Wang, J. Sun, J. Berberich, G. Wang, F. Allgöwer, and J. Chen, "Data-driven control of dynamic event-triggered systems with delays," *Int. J. Robust Nonlinear Control*, vol. 33, no. 12, pp. 7071–7093, 2023.

[18] X. Wang, J. Sun, G. Wang, F. Allg ower, and J. Chen, "Data-driven control of distributed event-triggered network systems," *IEEE/CAA J. Autom. Sinica*, vol. 10, no. 2, pp. 351–364, Feb. 2023.

[19] H. J. van Waarde, J. Eising, M. K. Camlibel, and H. L. Trentelman, "A behavioral approach to data-driven control with noisy input-output data," *IEEE Trans. Autom. Control*, vol. 69, no. 2, pp. 813–827, Feb. 2024.

[20] W.-L. Qi, K.-Z. Liu, R. Wang, and X.-M. Sun, "Data-driven $\mathcal{L}_2$-stability analysis for dynamic event-triggered networked control systems: A hybrid system approach," *IEEE Trans. Ind. Electron.*, vol. 70, no. 6, pp. 6151–6158, Jun. 2023.

[21] L. Huang, J. Coulson, J. Lygeros, and F. Dörfler, "Decentralized data-enabled predictive control for power system oscillation damping," *IEEE Trans. Control Syst. Technol.*, vol. 30, no. 3, pp. 1065–1077, May 2022.
[22] S. Buso and P. Mattavelli, *Digital Control in Power Electronics*. San Rafael, CA, USA: Morgan & Claypool, 2015.
[23] T. Dragičević, X. PLX, J. C. Lu, Vasquez, and J. M. Guerrero, "DC microgrids—Part II: A review of power architectures, applications, and standardization issues," *IEEE Trans. Power Electron.*, vol. 31, no. 5, pp. 3528–3549, May 2016.
[24] D. Das, N. Kumaresan, V. Nayanar, K. Navin Sam, and N. Ammasai Gounden, "Development of BLDC motor-based elevator system suitable for DC microgrid," *IEEE/ASME Trans. Mechatron.*, vol. 21, no. 3, pp. 1552–1560, Jun. 2016.
[25] M. Mosayebi, S. M. Sadeghzadeh, M. Gheisarnejad, and M. H. Khooban, "Intelligent and fast model-free sliding mode control for shipboard DC microgrids," *IEEE Trans. Transport. Electrific.*, vol. 7, no. 3, pp. 1662–1671, Sep. 2021.
[26] J. Loranca-Coutiño, J. C. Mayo-Maldonado, G. Escobar, T. M. Maupong, J. E. Valdez-Resendiz, and J. C. Rosas-Caro, "Data-driven passivity-based control design for modular DC microgrids," *IEEE Trans. Ind. Electron.*, vol. 69, no. 3, pp. 2545–2556, Mar. 2022.
[27] P. Manganiello, M. Balato, and M. Vitelli, "A survey on mismatching and aging of PV modules: The closed loop," *IEEE Trans. Ind. Electron.*, vol. 62, no. 11, pp. 7276–7286, Nov. 2015.
[28] W. Yao, X. Wang, P. C. Loh, X. Zhang, and F. Blaabjerg, "Improved power decoupling scheme for a single-phase grid-connected differential inverter with realistic mismatch in storage capacitances," *IEEE Trans. Power Electron.*, vol. 32, no. 1, pp. 186–199, Jan. 2017.
[29] R. W. Erickson and D. Maksimovic, *Fundamentals of Power Electronics*. Berlin, Germany: Springer, 2007.
[30] K. Rouzbehi, A. Miranian, J. M. Escaño, E. Rakhshani, N. Shariati, and E. Pouresmaeil, "A data-driven based voltage control strategy for DC-DC converters: Application to DC microgrid," *Electronics*, vol. 8, no. 5, 2019, Art. no. 493.
[31] L. Cupelli, M. Cupelli, and A. Monti, "Data-driven control of converters in DC microgrids for bus voltage regulation," in *Proc. 44th Ann. Conf. IEEE Ind. Electron. Soc.*, 2018, pp. 3389–3394.
[32] S. S. Madani and A. Karimi, "Data-driven robust passivity-based controller design for grid-connected converters," *IEEE Trans. Control Syst. Technol.*, vol. 32, no. 2, pp. 300–310, Mar. 2024.
[33] L. Huang, J. Coulson, J. Lygeros, and F. Dörfler, "Data-enabled predictive control for grid-connected power converters," in *Proc. IEEE 58th Conf. Decis. Control*, 2019, pp. 8130–8135.
[34] W. Yu, Z. Tang, and W. Xiong, "Distributed robust data-enabled predictive control based voltage control for networked microgrid system," *Electric Power Syst. Res.*, vol. 231, 2024, Art. no. 110360.
[35] A. Bisoffi, C. De Persis, and P. Tesi, "Trade-offs in learning controllers from noisy data," *Syst. Control Lett.*, vol. 154, 2021, Art. no. 104985.
[36] H. J. van Waarde, M. K. Camlibel, J. Eising, and H. L. Trentelman, "Quadratic matrix inequalities with applications to data-based control," *SIAM J. Control Optim.*, vol. 61, no. 4, pp. 2251–2281, 2023.
[37] F. Mumtaz, N. Zaihar Yahaya, S. Tanzim Meraj, B. Singh, R. Kannan, and O. Ibrahim, "Review on non-isolated DC-DC converters and their control techniques for renewable energy applications," *Ain Shams Eng. J.*, vol. 12, no. 4, pp. 3747–3763, 2021.
[38] M. S. Sadabadi, Q. Shafiee, and A. Karimi, "Plug-and-play robust voltage control of DC microgrids," *IEEE Trans. Smart Grid*, vol. 9, no. 6, pp. 6886–6896, Nov. 2018.

Zi-Jie Wei received the B.S. and M.S. degrees in electrical engineering and automation, in 2018 and 2022, respectively, from the Dalian University of Technology, Dalian, China, where he is currently working toward the Ph.D. degree in control theory and engineering.

His research interests include networked control systems, data-driven analysis and control, and dc microgrid control.

Kun-Zhi Liu received the bachelor's degree in automation from the Harbin University of Science and Technology, Harbin, China, in 2011, and the master's and Ph.D. degrees in control science and engineering from the Dalian University of Technology, Dalian, China, in 2013 and 2017, respectively.

He is currently a Professor with the School of Control Science and Engineering, Dalian University of Technology. His main research interests include hybrid systems, delay systems, cyber-physical systems, and data-driven control.

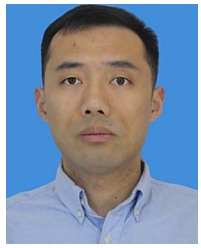

Ping Lin (Member, IEEE) received the Ph.D. degree in navigation guidance and control from the School of Control Science and Engineering, Dalian University of Technology, Dalian, China, in 2021.

From 2022 to 2024, he was working as a Postdoctoral Researcher with the Dalian University of Technology. He is currently an Associate Professor with the School of Control Science and Engineering, Dalian University of Technology, Dalian, China, since 2024. His research interests include nonlinear systems, active disturbance rejection control, and generator control systems.

Xi-Ming Sun (Senior Member, IEEE) received the M.S. degree in applied mathematics from Bohai University, Jinzhou, China, in 2003, and the Ph.D. degree in control theory and control engineering from Northeastern University, Shenyang, China, in 2006.

From 2006 to 2008, he was a Research Fellow with the Faculty of Advanced Technology, University of Glamorgan, Pontypridd, U.K. He then Visited the School of Electrical and Electronic Engineering, Melbourne University, Melbourne, VIC, Australia, in 2009, and the Polytechnic Institute of New York University, New York, NY, USA, in 2011. He is currently a Professor of control theory and control engineering with the School of Control Science and Engineering, Dalian University of Technology, Dalian, China. His research interests include aero-engine control, switched delay systems, networked control systems, and nonlinear systems.

Dr. Sun was the recipient of the Most-Cited Article 2006–2010 Award from *Automatica* in 2011. He has been an Associate Editor for IEEE TRANSACTIONS ON CYBERNETICS since 2014.